JOURNAL OF MATERIALS SCIENCE 22 (1987) 4504–4513

Growth mechanisms of modified eutectic silicon

J. M. DOWLING*‡, J. M. CORBETT‡, H. W. KERR*
*Department of Mechanical Engineering, University of Waterloo, Waterloo, Ontario, Canada and ‡Guelph–Waterloo Program for Graduate Work in Physics – Waterloo Campus, University of Waterloo, Waterloo, Ontario, Canada, N2L 361

Transmission electron microscopy has been used to study the growth mechanism of silicon in modified aluminium–silicon eutectic alloys. In agreement with earlier studies a high density of thin {1 1 1} faults was observed in silicon modified by relatively large amounts of sodium or strontium. High-resolution microscopy showed that these faults were a mixture of thin twins and stacking faults, the inter-fault spacing being at least ten times the twin width. Because modified silicon is thought to grow by the twin re-entrant edge mechanism, the thin twins were examined in relation to the shape of the modified silicon dendrites and the solidified growth interfaces. It was concluded that the thin faults were not deformation twins resulting from either thermal contraction stresses or mechanical grinding during specimen preparation. No direct evidence was found to support the re-entrant edge mode of growth in modified silicon. Instead it is suggested that the interface may appear macroscopically non-faceted, as in the more general Lateral Microscopic Growth mechanisms.

1. Introduction

The modification of silicon in aluminium–silicon alloys from flake to more fibrous forms was first described over 60 years ago. In the original work the modification was caused by sodium additions. Subsequent work has shown that modification may also be brought about by strontium additions or simply by rapid solidification. The modification has important industrial implications, because it results in a significant increase in strength. Many researchers have therefore studied the modification phenomenon, and have suggested reasons for it. Despite the time span since its discovery, disagreements about the modification process still exist. In particular, it is not clear whether the modified silicon solidifies with a non-faceted solid–liquid interface or a faceted interface. Flood and Hunt [1] suggested that in castings, sodium-modified silicon grows with a non-faceted interface, permitting finer spacings than in the unmodified alloys in which the silicon is faceted. This proposal is in contrast to earlier studies on sodium-modified [2] and quench-modified [3] silicon. In these studies, thin faults identified as twins were observed in the silicon using transmission electron microscopy. Growth and morphology of the modified silicon was attributed to the twin re-entrant edge model [4] and the solid–liquid interface was assumed to be faceted. Two more recent publications also report the presence of twins in both sodium-modified [5] and strontium-modified [6] silicon and an increase in twin density over the quench-modified material. Again, the silicon is assumed to grow by the re-entrant edge mechanism with a faceted interface.

Despite these recent reports, the evidence for faceted growth aided by twins in these alloys is not yet proven, and various questions remain unanswered. It is clear that there are very thin planar defects within the modified silicon of both the earlier and recent studies. Although sodium-modified and strontium-modified silicon contained faults which formed twin spots in electron diffraction [5, 6], diffraction streaks along ⟨1 1 1⟩ were also present in the sodium-modified material and these imply either very thin twins or stacking faults [5]. Because neither dark-field imaging nor lattice imaging were presented in the latter report, the exact nature of the faults is uncertain. The solidified interfaces of the silicon also present evidence against faceted growth because these surfaces are curved and lack the crystallographic outlines associated with faceted growth. Indeed in Lu and Hellawell's paper [5], it is noted that sodium-modified silicon is "somewhat" faceted but that faceting is less pronounced in highly twinned material.

To clarify the nature of the faults and the shape of the growth interfaces, aluminium–silicon alloys have been studied using transmission electron microscopy. The observations have been interpreted and discussed in relation to solidification mechanisms.

2. Methods and materials

2.1. Materials

Molten aluminium–silicon alloys, close to the binary eutectic composition, were drawn into a narrow-bore glass tube of at least 3 mm diameter and then solidified under different cooling conditions, with and without the modifying agents strontium and sodium. Alloys without the modifying agents were prepared in both the quenched (Q) and the air-cooled (A) condition.

0022–2461/87 $03.00 + .12

TABLE I Solidification data and alloy compositions

Alloy*	Si (wt %)	Modifying agent	Casting temperature (°C)	Cooling rate
D-Na	8.6	0.01 wt % Na	955	Directionally solidified: 1.125 mm sec^{-1}
D-Sr	8.5	0.04 wt % Sr	950	Directionally solidified: 1.156 mm sec^{-1}
Q	12.6	None added	750	Quenched
A	12.6	None added	750	Air-cooled
A-Na	12.6	0.06 wt % Na	730	Air-cooled

*Impurities as follows: Cu, Mg, Zn, Pb, Cr, Mn, Ti, Sn all less than 0.01 wt %; Fe ca. 0.12 wt %; Ni ca. 0.01 wt %.

Sodium-modified material was prepared in the air-cooled and directionally solidified states whilst strontium-modified alloys were prepared only in the directionally solidified (D) state. The alloy compositions and solidification data are given in Table I.

2.2. Transmission electron microscopy (TEM)

TEM specimens were prepared by a deep-extraction technique. Small pieces of alloy were immersed in a 2% solution of hydrochloric acid, which slowly dissolved the aluminium matrix releasing the silicon to form a grey sediment. Every few days the sediment was removed and washed several times in water, whilst the remainder of the specimen was returned to a fresh acid bath. Thus for each alloy a series of silicon extractions was obtained. Droplets of the extractions, suspended in an ethanol and water mixture, were placed on carbon support films on copper grids.

For Alloys Q and A-Na, additional specimens were prepared by electrolytically jetting thin 3 mm discs (previously ground) with a solution of 30% HNO_3 in methanol at room temperature. The jetted discs each contained several perforations where the acid had dissolved the aluminium. Silicon crystals, embedded in the remaining alloy, protruded into the holes.

The silicon crystals were examined in a Philips EM300 operated at 100 kV. The crystals were studied in bright field and centred dark field at $\langle 1\,1\,0 \rangle$ zone axis orientations and at other major zone axes.

Samples of extracted silicon from the sodium-modified and strontium-modified alloys were also examined at 250 kV in a Philips EM430. Where crystal thickness permitted, high-resolution images of the crystal structure and defects were obtained.

3. Observations

3.1. General trends in silicon morphology

Modification of the silicon phase, by either chemical means or quenching, changed the morphology from plates to dendrites (Fig. 1). In the quench-modified and low-sodium (0.01 wt %) alloys, the dendrites were fibrous with round or curved outlines but became more angular and faceted with larger additions of sodium or strontium (Table II and Fig. 1).

Regardless of the modification agent, all the silicon dendrites were highly branched (Fig. 1). Examination of the dendrites, at different zone axis orientations, showed that the branches were not rods but had zigzag or corkscrew shapes. The faceted sides and edges in all the modified alloys tended to be parallel to $\{1\,1\,1\}$ planes or $\langle 1\,1\,0 \rangle$ intersections of $\{1\,1\,1\}$ planes (Figs 1a and b).

The symmetry or growth axes for the dendrite spines were either $\langle 1\,0\,0 \rangle$ or $\langle 1\,1\,0 \rangle$ in chemically modified silicon but $\langle 1\,1\,0 \rangle$ or $\langle 1\,1\,2 \rangle$ in the quench-modified material. The symmetry axes were $\langle 1\,1\,0 \rangle$ and $\langle 1\,1\,2 \rangle$ for the straight-sided segments in all dendrite branches. For entirely irregular and zigzag branches, no rational or consistent growth axes were observed.

3.2. Twins, microtwins and stacking faults

Modification changed not only the external shape of the silicon but also the nature, size and distribution of faults on $\{1\,1\,1\}$ planes (Table II). Whereas in unmodified (A) silicon there were large thick twins, such defects were very rare in the quenched and chemically modified crystals. Conversely, very thin twins and stacking faults were common features of

TABLE II Effects of modification on the appearance of silicon

Alloy	Modification	Morphology	Outline	Branch tips	Branch sides	Thick twins	Thin twins or stacking faults
A	None: air-cooled	Plates	Round edges	–	–	Width $\geqslant 0.1\,\mu m$	None
Q	Quenched	Dendrites	Fibrous + curved	Mostly round	Curved + faceted	Rare	Yes; spacing = 0.025 μm, spacing/width = 25 : 1
D-Na	0.01 wt % Na	Dendrites	Fibrous + curved	Mostly round	Curved + faceted	Rare	Yes; spacing = 0.025 μm, spacing/width = 25 : 1
A-Na	0.06 wt % Na	Dendrites	Faceted + angular	Mixed: wavy + faceted	Faceted + curved	Rare	Yes; spacing = 0.01 μm, spacing/width = 10 : 1
D-Sr	0.04 wt % Sr	Dendrites	Faceted + angular	Mixed: wavy + faceted	Faceted + curved	Rare	Yes; spacing = 0.01 μm, spacing/width = 10 : 1

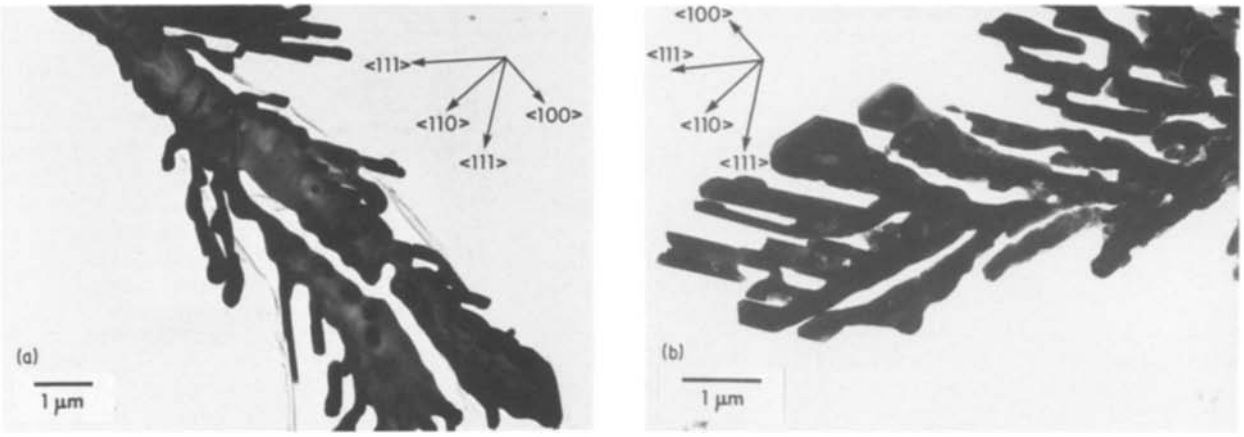

Figure 1 Dendritic silicon from chemically modified alloys; ⟨1 1 0⟩ zone axis. (a) 0.01 wt % sodium addition (Alloy D-Na). (b) 0.04 wt % strontium addition (Alloy D-Sr).

modified dendritic silicon but were not present in the unmodified plates.

In the unmodified silicon, the {1 1 1} twin planes were parallel to the plane of the plate. These faults were only clearly visible when the plane of the plate was parallel to the electron beam and the zone axis orientation was ⟨1 1 0⟩. With these conditions, the presence of the twins was confirmed by the presence of twin spots in the diffraction patterns and by centred dark-field imaging (Fig. 2). The plate in Fig. 2 contained several twin/matrix layers and these ranged in width from about 0.1 to 0.5 μm, i.e. the twin and matrix were of roughly equal width. Across the thickness of the plate, the edge profile undulates with no faceting in either matrix or twin layers.

Large thick twins like those shown in Fig. 2 were rarely seen in the modified dendrites. When dendrites yielded diffraction patterns with twin spots, the material in the twin orientation was only in a small section of a branch (Fig. 3). Wide twins were never seen along the entire lengths of branches or central spines.

Very thin planar defects on {1 1 1} planes were present in all the modified silicon dendrites and, in diffraction, these faults gave rise to very long streaks through {1 1 1} reflections (Figs 3 and 4). Because both thin twins (microtwins) and stacking faults form long diffraction streaks, these defects are only distinguishable at high resolution. Examination at 250 kV showed that the modified silicon contained both very thin twins and stacking faults (Fig. 5), the thin twins being only a few atoms thick (1 to 2 nm).

The distribution of the thin defects was patchy in both quench- and chemically-modified dendrites but there were clearly fewer {1 1 1} faults in quenched and 0.01 wt % sodium-modified silicon than in 0.06 wt % sodium- and 0.04% strontium-modified materials (cf. Figs 3, 4 and 6). In quenched silicon and the 0.01 wt % sodium alloy, average fault spacings were of the order of 0.025 μm with individual spacings

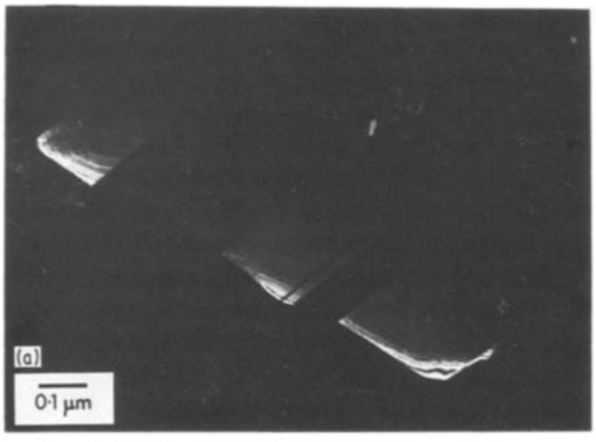

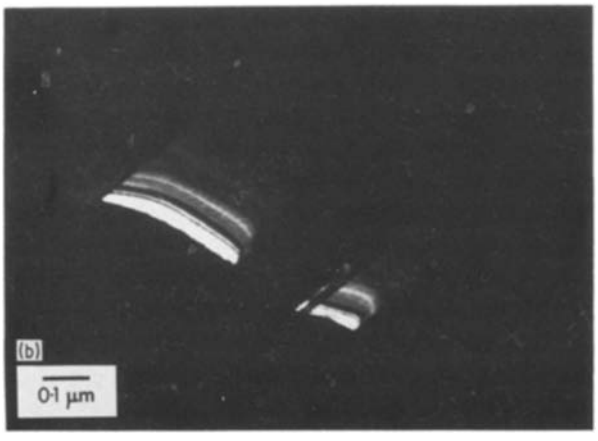

Figure 2 Thick twins in plate silicon from unmodified, air-cooled Alloy A; ⟨1 1 0⟩ zone axis. (a) Centred dark-field image using Spot A in Fig. 2c. (b) Centred dark-field image using Spot B in Fig. 2c. (c) Diagram of ⟨1 1 0⟩ pattern for Figs 2a and b: the image-pattern rotation has been corrected.

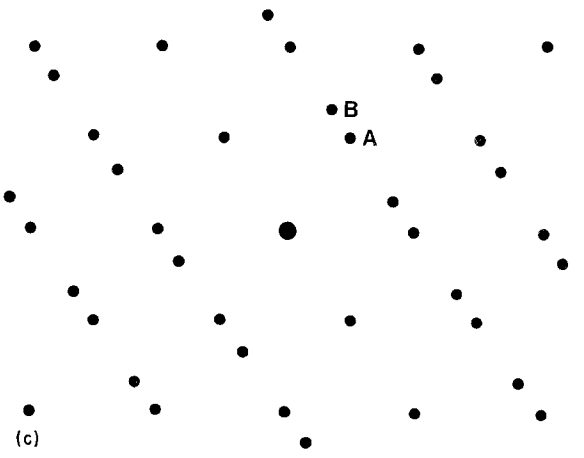

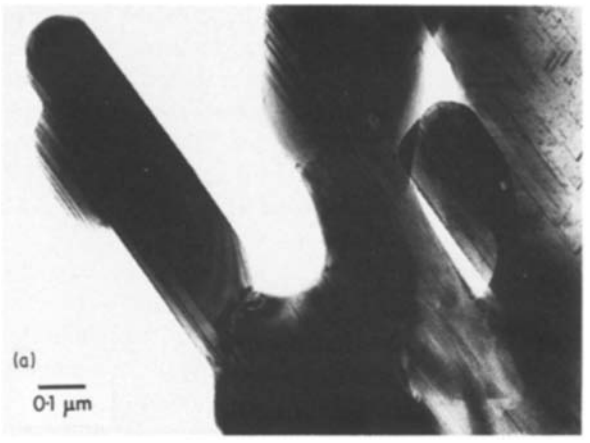

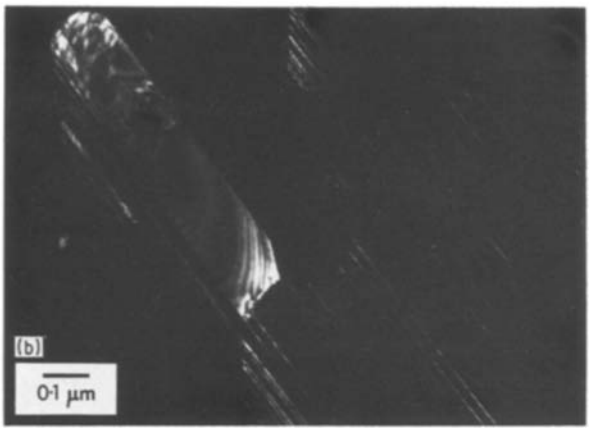

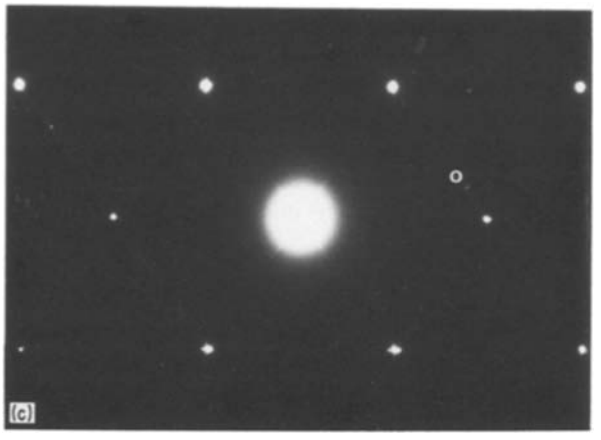

Figure 3 Thick twins in the sodium-modified dendrite shown in Fig. 2a. (a) Bright-field image. (b) Centred dark-field image using the marked twin spot in Fig. 3c. Thin twins are visible as well as the thick twins because the objective aperture covered part of the $\langle 1\,1\,1 \rangle$ streak. (c) $\langle 1\,1\,0 \rangle$ diffraction pattern: Fig. 3b was formed using the marked faint spot. (Image-pattern rotation has not been corrected).

ranging from 0.005 to 0.1 μm in many branches. For the strontium and 0.06% sodium alloys, the fault spacings were approximately 0.01 μm in many branches but individual spacings of up to 0.05 μm were not uncommon. These inter-fault spacings were larger than the thin faults by an order of magnitude. The ratio of fault spacing to width was about 25 : 1 in quenched and low sodium alloys and 10 : 1 in the high sodium and strontium ones.

Each dendrite usually contained thin twins on more than one $\{1\,1\,1\}$ plane. In the dendrite spines at least two sets were present and these lay diagonally with respect to the $\langle 1\,0\,0 \rangle$ and $\langle 1\,1\,0 \rangle$ symmetry axes of the spines (Fig. 6). Within an individual branch, there was usually a dominant set of twins on one $\{1\,1\,1\}$ plane but in some segments there were a few twins on another $\{1\,1\,1\}$ plane. The dominant set lay along the length of the branch segments whilst the minority set were on the diagonal. Segments containing only one major set of thin twins had sides parallel to the twin plane (Figs 3, 4 and 6). Segments with roughly equal numbers of faults on two (1 1 1) planes had bulbous sides (Fig. 4b).

3.3. Tips of branches

At relatively low magnifications, the branch tips or growing ends presented a variety of profiles. In the quench-modified dendrites and also the 0.01 wt %

Figure 4 Thin $\{1\,1\,1\}$ fault distribution in modified silicon; $\langle 1\,1\,0 \rangle$ zone axis. (a) Quench-modified Alloy Q. (b) Strontium-modified Alloy D-Sr.

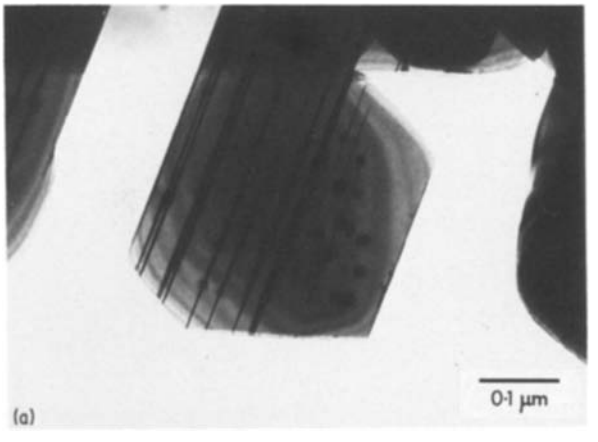

sodium-modified material, the tips had round or wavy profiles with the occasional facet (Figs 1, 3 and 4). A higher incidence of faceted tips was observed in the 0.06 wt % sodium and 0.04 wt % strontium alloys but wavy and irregular outlines were also common (Figs 1 and 4). The tip facets were often parallel to {1 1 1} planes or ⟨1 1 0⟩ intersections of {1 1 1} planes, but there were also crystallographic outlines which were not parallel to any low-index plane.

Although many of the thin twins and stacking faults appeared to intersect the surfaces of the branch tips, no microscopic steps or serrations were visible at the intersections (Fig. 4). High-resolution imaging confirmed this lack of microscopic indents and serrations at the tip surfaces (Fig. 5). At these very high magnifications, it was also evident that some {1 1 1} defects stopped short of the surface.

4. Discussion

4.1. Silicon morphology and twins

The macroscopic appearance of the unmodified material was in agreement with observations in other studies [5, 6]. The round, fibrous nature of quench-modified dendrites and the more angular and faceted shape of the high-sodium and strontium-modified silicon has also been observed by other authors [5].

Highly branched dendrites were a striking characteristic of the strontium and high-sodium alloys (Fig. 1). Branching was so extensive in some dendrites that it was difficult to see the {1 1 1} faults because of overlapping branches. This observation is contrary to other reports on sodium-modified silicon where the dendrites were described as mostly branchless [5]. In the studies reported here, extracted silicon crystals were used. The specimens used by Lu and Hellawell [5] were electrochemically jetted discs where the

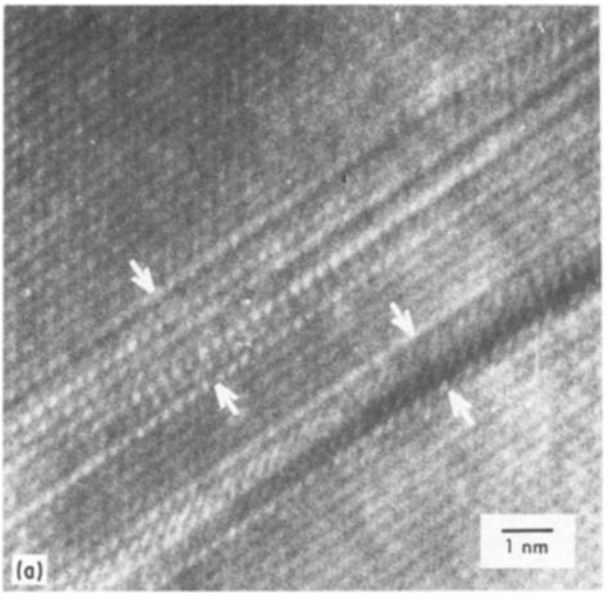

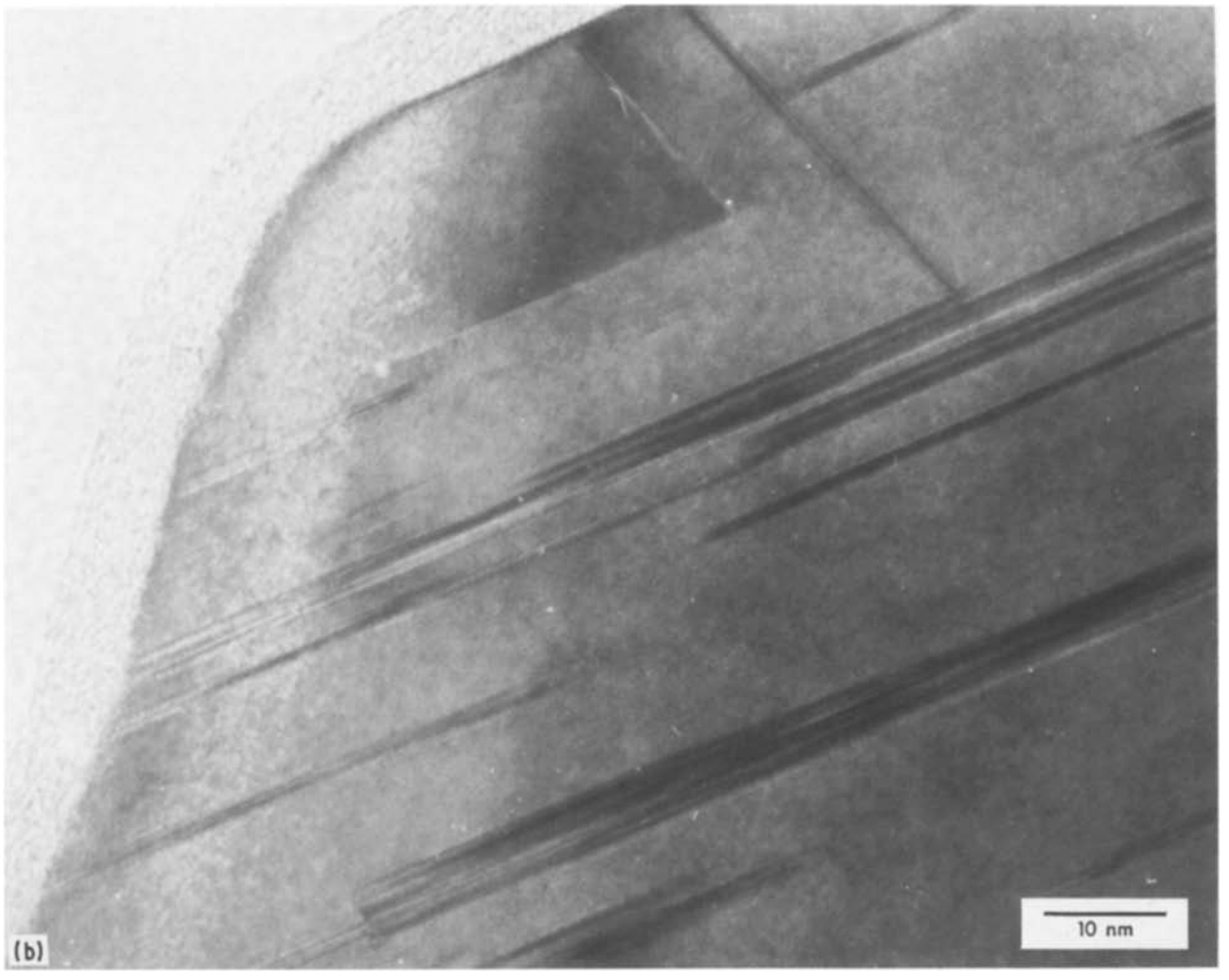

Figure 5 Lattice images of modified silicon alloys; ⟨1 1 0⟩ zone axis. (a) Thin twins and stacking faults (indicated by arrows). (b) Branch tip.

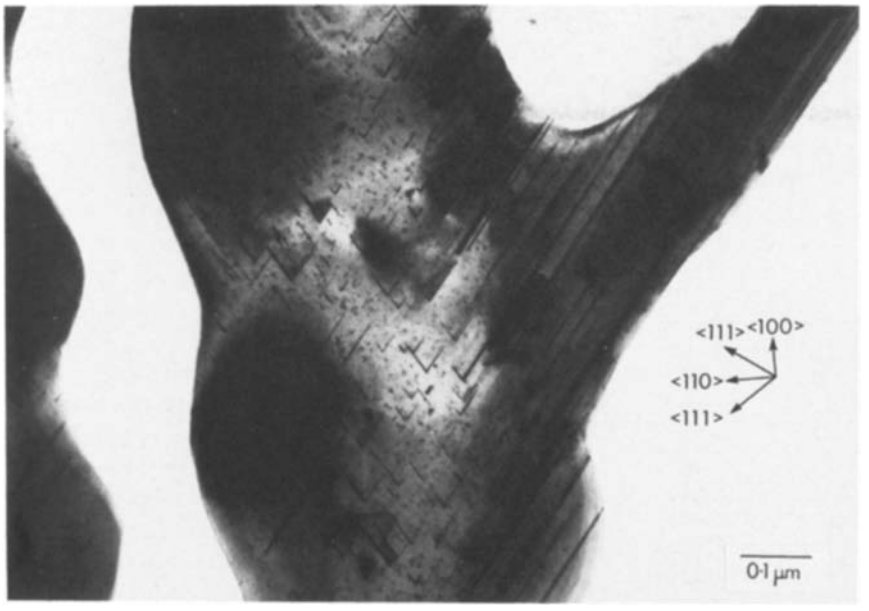

Figure 6 Orientation and discontinuous nature of {1 1 1} faults in spine and branches of the dendrite in Fig. 2a.

silicon dendrites protruded into holes left by dissolution of the aluminium. To investigate the possibility that branchless fibres were being lost during deep extraction, jetted discs of Alloys Q and A-Na were examined. Very few branchless dendrites were seen in these specimens. Therefore it was concluded that the branched dendrites were representative of the alloys. The difference in the degree of branching between the two studies may have been influenced by the impurity levels of the alloys used. The unbranched silicon of earlier studies was obtained from a high-purity alloy (60 p.p.m. total impurity) whereas the highly branched dendrites described here were from commercially pure material (Table I). This increase in impurity level perhaps promoted a cellular or dendritic growth morphology. The silicon content was apparently not important because highly branched dendrites were seen in both 8.6% and 12.6% modified alloys in this study.

With regard to the thin faults on {1 1 1} planes, many authors have reported on their nature and distribution in quench- and chemically-modified silicon. The observed increase in fault density and the presence of faults on more than one {1 1 1} plane in chemically-modified alloys was consistent with earlier studies [2, 5, 6]. However, the faults have previously been referred to as twins even though the evidence, long diffraction streaks, was ambiguous: both thin twins and stacking faults form streaks. More recently [5, 6], discrete twin spots have been observed in diffraction patterns from sodium- and strontium-modified dendrites and this would seem to supply hard evidence for calling the faults twins. But the diffraction patterns from the sodium-modified material [5] also contained streaks along ⟨1 1 1⟩ and these imply the presence of thin faults in addition to the thicker ones forming twin spots.

In the present study, discrete twin spots were rarely seen and high-resolution imaging showed that the defects were stacking faults or thin twins, just a few atoms thick. The few thick twins which formed twin spots were only seen in isolated segments and were never uniformly distributed throughout the dendrite. Random ⟨1 1 0⟩ examinations of many dendrites should yield twin spots in at least 50% of the patterns if thicker twins were consistently present in the silicon. Because only one or two patterns with twin spots were seen, it was concluded on the whole that dendrites contained only very thin twins or stacking faults.

The question arises whether or not the thin {1 1 1} faults are artefacts of the specimen preparation procedure. Formation of thin twins, as a result of mechanical damage to the silicon surface, is well documented [7, 8]. Polishing with either alumina or diamond paste is known to produce thin twins in silicon [7]. However, the silicon crystals in this study were prepared by deep extraction and samples were taken from the central parts of the bulk alloys, well away from any sawn or outer surfaces. In addition, microtwins and stacking faults were not seen in the unmodified silicon plates which were prepared by the same method. Therefore the authors are confident that the planar {1 1 1} faults are inherent to the modified dendrites and are not introduced during specimen preparation.

Formation of deformation twins as a result of thermal stresses was also considered. Bulk silicon has a smaller coefficient of expansion than aluminium and will be in compression at low temperatures. For very long thin cylindrical rods embedded in another media, the compressive thermal stresses are axisymmetric and thus the shear stresses τ_{rz} and τ_{zr} on the principal planes are zero [9]. Hence, if the effects of anisotropy are ignored for silicon dendrites in aluminium, the shear stresses will be zero on the {1 1 1} planes parallel to the branch sides. Thus the long thin faults on these {1 1 1} planes must be inherent to the growth of the dendrites.

The twins at an angle to the branch sides also need to be considered. The maximum thermal shear stress τ_{max} inside an embedded rod can be calculated from $\tau_{max} = 0.5\ (\sigma_r - \sigma_z)$ where σ_r and σ_z are the radial and axial stresses in the rod [9]. σ_r, σ_z and τ_{max} are not functions of rod diameter. However, they are

TABLE III Calculated thermal shear stresses within silicon rods embedded in aluminium*

Stress	R_1/R_2					
	0.9	0.8	0.6	0.5	0.2	0.1
τ_{max} (MPa)	62	128	263	328	476	506
$\tau_{112/110}$ (MPa)	58	120	247	308	448	476
$\tau_{112/112}$ (MPa)	49	101	207	258	374	397

Parameters used to calculate τ_{max}
Poisson's ratio: Si 0.3, Al 0.34
Young's modulus (GPa): Si 113, Al 71
Linear coefficient of expansion (K^{-1}): Si 3×10^{-6}, Al 23×10^{-6}
Temperature drop = $T_2 - T_1 = 557$ K where $T_2 = 850$ K and $T_1 = 293$ K

*R_1 = radius of silicon rod, R_2 = radius of rod plus surrounding aluminium envelope, τ_{max} = maximum shear stress calculated using [9], $\tau_{112/110}$ = largest resolved shear stress for $\langle 1\,1\,2\rangle$ shear on $\{1\,1\,1\}$ inclined to $\langle 1\,1\,0\rangle$ symmetry axis, $\tau_{112/112}$ = largest resolved shear stress for $\langle 1\,1\,2\rangle$ shear on $\{1\,1\,1\}$ inclined to $\langle 1\,1\,2\rangle$ symmetry axis.

inversely proportional to the ratio R_1/R_2 of rod radius (R_1) to rod plus envelope radius (R_2). Table III contains calculated values of τ_{max} for a range of R_1/R_2 values for silicon rods embedded in aluminium. In a branch segment of a silicon dendrite, the $\{1\,1\,1\}$ shear planes for twinning will not be parallel to those of the maximum stress because the segment symmetry axes are either $\langle 1\,1\,0\rangle$ or $\langle 1\,1\,2\rangle$. Included in Table III are maximum values of the calculated shear stresses for $\langle 1\,1\,2\rangle/\{1\,1\,1\}$ deformation twinning for the two symmetry axes. For branch segments which nearly touch ($R_1/R_2 = 0.9$), the $\langle 1\,1\,2\rangle$ shear stresses are 50 to 60 MPa but rise to 400 to 475 MPa for widely spaced branches where $R_1/R_2 = 0.1$. These calculated values are all less than the experimental value of 493 MPa at 450° C required to generate twins from hardness indentations in silicon, the shear stress being applied for 2.5 h [10]. Since most dendrites had closely spaced branches with $R_1/R_2 > 0.5$ and hence shear stresses less than 300 MPa, it seems likely that diagonal thin twins were formed during branch growth. Although indents in the branches may locally increase shear stresses, it is unlikely that this will be sufficient to induce twinning considering the laboratory conditions required to generate twins [10]. Moreover, many of the observed diagonal twins are not close to any local indentations or jogs on the branch (Figs 4 and 6). Hence we conclude that the modified silicon contains both microtwins and stacking faults which were formed during solidification.

4.2. Growth mechanisms

Recently it has been re-proposed that twin re-entrant edge growth is the operative growth mechanism for fibrous silicon in sodium-modified [5] and strontium-modified eutectics [6]. The arguments and evidence put forward to support this view hinge on the high density of $\{1\,1\,1\}$ faults, and kinetic considerations such as undercoolings and growth rates.

The twin re-entrant edge mechanism was originally invoked to describe the shape of single-crystal dendrites of germanium grown from the melt [4]. A seed crystal containing at least two $\{1\,1\,1\}$ twin planes was withdrawn along a $\langle 1\,1\,2\rangle$ direction in the twin plane. Crystal growth was then facilitated by two-dimensional nucleation along the grooves between twin and matrix with subsequent lateral spreading along the $\{1\,1\,1\}$ faces of the twins and matrix. The details of the growth crystallography are often presented by considering a thin $\langle 1\,1\,0\rangle$ section through the growing plate as shown in Fig. 7 [4]. The main geometric and crystallographic points are that the growing front is macroscopically faceted, and that facets in both twin and matrix are $\{1\,1\,1\}$ planes perpendicular to the plane of the section. The twin planes are perpendicular to the section but also parallel to the sides of the crystal. The apparent macroscopic growth direction is then a $\langle 1\,1\,2\rangle$ lying in the twin plane. Twins and matrix are assumed to be of similar widths and to grow at similar rates such that the macroscopic growth front is perpendicular to the $\langle 1\,1\,2\rangle$ growth direction.

If the above description is correct, then the growing ends of the silicon branches should have nicely faceted tips bounded by $\{1\,1\,1\}$ planes in the $\langle 1\,1\,0\rangle$ orientation. It is immediately apparent that virtually no branch tips in either quench- or chemically-modified silicon resembled the geometry in Fig. 7. On the other hand, round, wavy and triangular ends were common (Figs 1, 3 and 4). Admittedly, at low magnifications, microfaceting across the thin faults will not be visible but even in lattice images (Fig. 5) no serrations or facets were visible.

The lack of faceting conceivably may have resulted from the specimen preparation, the deep extractions requiring several days. However, silicon crystals extracted in under 2 days were similar in appearance to those left in acid for 14 days, i.e. there was no increase in the incidence of round profiles. Indeed, any acid attack would be expected to lead to more

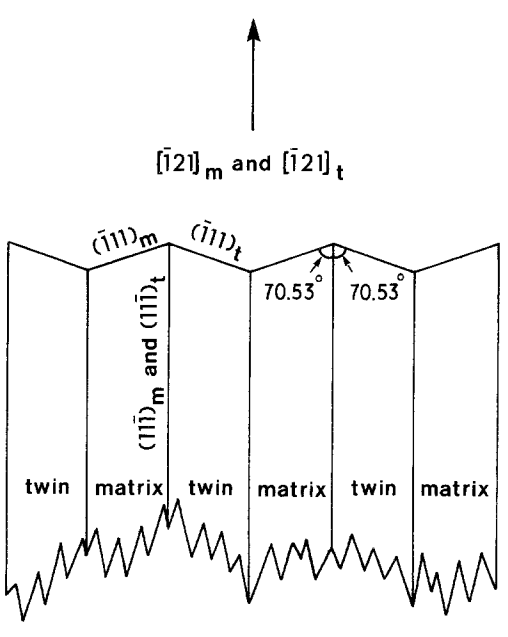

Figure 7 The geometry of twin re-entrant edge growth (based on [4]).

faceting, because prolonged etching of bulk silicon usually reveals the low-energy {1 1 1} planes.

Precipitation of silicon on to the branch tips after solidification may have perhaps altered the original faceted solid–liquid interface. However, both the quench-modified and slowly solidified chemically-modified silicon showed similar shapes, despite great differences in the amount of time available for deposition of silicon from the solid. Moreover it would require substantial amounts of silicon deposition to change the facets to curves and, in any case, solid-state precipitation is expected to enhance faceting. Retrospective studies of the silicon branch tips were deemed therefore to provide a reliable view of the original growing interfaces.

The observed profiles of the branch tips will be modified by the exact choice of ⟨1 1 0⟩ orientation used to reveal the twins. For a perfect single crystal the ⟨1 1 0⟩ orientations are equivalent, but for a silicon crystal with {1 1 1} faults the appearance of these defects and their intersections with surfaces will change with the selected ⟨1 1 0⟩. Another consideration is the three-dimensional nature of the dendrites and the effect this has on the observed profiles. The resulting image is no longer a projection of a very thin slice as shown in Fig. 7. Instead, the image will be a projection of the whole crystal and the external morphology and crystal thickness will modify and obscure detail.

The effects of the above considerations were studied by looking at the different ⟨1 1 0⟩ orientations for a silicon branch tip bounded by {1 1 1} surfaces. The tip was assumed to have a growth front made up of {1 1 1} planes in both twins and matrix, the twin planes being parallel to one of the {1 1 1} sides (Fig. 8). The relative thicknesses of the twins and matrix in Fig. 8 were chosen to reflect the observed spacings in the silicon dendrites, i.e. the interfault spacings were much larger than the fault widths. Essentially, the ⟨1 1 0⟩ images fell into two groups, one where the {1 1 1} faults were edge-on to the beam and the other where they were inclined.

For simplicity only the ⟨1 1 0⟩ orientations with edge-on {1 1 1} faults will be considered. In this group, the predicted growing tip shapes were always serrated in very thin sections and the serrations persisted in the three-dimensional projections of the whole crystal. Depending on the orientation of the tip planes with respect to the beam, the tip serrations in both twin and matrix will appear parallel to either an edge-on {1 1 1} or a ⟨1 1 0⟩ intersection of two {1 1 1} planes (Fig. 8). If the tip develops two different {1 1 1} planes in both matrix and twin orientation, the regular serrations are replaced by uneven multifaceting. The profile of the tip will then be wavy (Fig. 8d).

It is clear that many of the branch tips in Figs 1, 3 and 4 resemble the wavy profile of Fig. 8d. However, these similarities do not provide irrefutable evidence of re-entrant edge growth and some other criteria must be sought. Direct evidence of faceting on {1 1 1} planes in twin and matrix would appear to provide a satisfactory criterion, but as discussed previously lattice imaging provided no evidence of faceting at the atomic level. A growth direction of ⟨1 1 2⟩ might appear to be a sufficient condition from Fig. 7, but for images in ⟨1 1 0⟩ orientations there is always a ⟨1 1 2⟩ direction along the {1 1 1} faults and in the plane of the image. This consistency in apparent growth direction is merely a consequence of choosing the ⟨1 1 0⟩ orientation to examine the dendrites. Thus from these crystallographic and geometric arguments, there is apparently no hard evidence to support re-entrant edge growth in silicon dendrites.

However, it may be naive to assume that a growth front will appear macroscopically or microscopically faceted just because a crystal grows by deposition of atom layers on to a preferred crystallographic plane. Studies of growth mechanisms in semiconductors have shown that silicon and other materials can grow with a macroscopically curved growth front, yet at the atomic level growth proceeds on low-index planes [11, 12]. In the Lateral Microscopic Growth model [11, 12] the growth interface is assumed to consist of a series of terraces, one or two atoms high. Each terrace consists of a flat tread and a vertical riser. The treads are slow-growth planes such as {1 1 1} or {1 0 0} but the risers are not necessarily specific crystallographic planes. Nucleation occurs preferentially at the base of the risers and lateral growth continues by movement of the risers across the underlying terraces. Growth normal to the low-index planes proceeds by superposition of laterally advancing terraces, called Perpendicular Macroscopic Growth [11]. The resulting solid–liquid interface is then composed of a series of steps at the atomic level, and may appear round because lateral spreading of one layer is not completed before the next one is initiated. This combination of riser and tread growth may account for the lack of macroscopic faceting at the branch tips and also in plate silicon. Twin re-entrant edge growth is then a special type of Perpendicular Macroscopic Growth where nucleation of new layers is aided by the twin–matrix groove. The growth of the silicon involves facets on the terraces, but not necessarily on the risers, so that the resulting shape does not appear faceted. It may then be misleading to take macroscopic faceting as a criterion of twin re-entrant edge growth.

Earlier papers [4–6] concluded that the presence of twins in modified silicon proved that re-entrant edge growth took place. Indeed, using the traditional and logical argument that the longest crystal dimension identifies the fastest or easiest growth direction, it must be accepted that the twins aid growth in the branches of the silicon dendrites. However, differences in twin orientation and density between spines and branches suggest that additional growth mechanisms operate. In dendrite spines, the faults were very short, terminating within the crystal and at an angle to the width (Figs 1a and 6). Only in the branches were the twins parallel to the growth direction, (Figs 3 and 6). Observations by Washburn [13] clarify details of atom addition on to advancing interfaces. In the transformation of amorphous to crystalline silicon, he observed that the growth sequence depended upon the crystallography of the growing interface. For

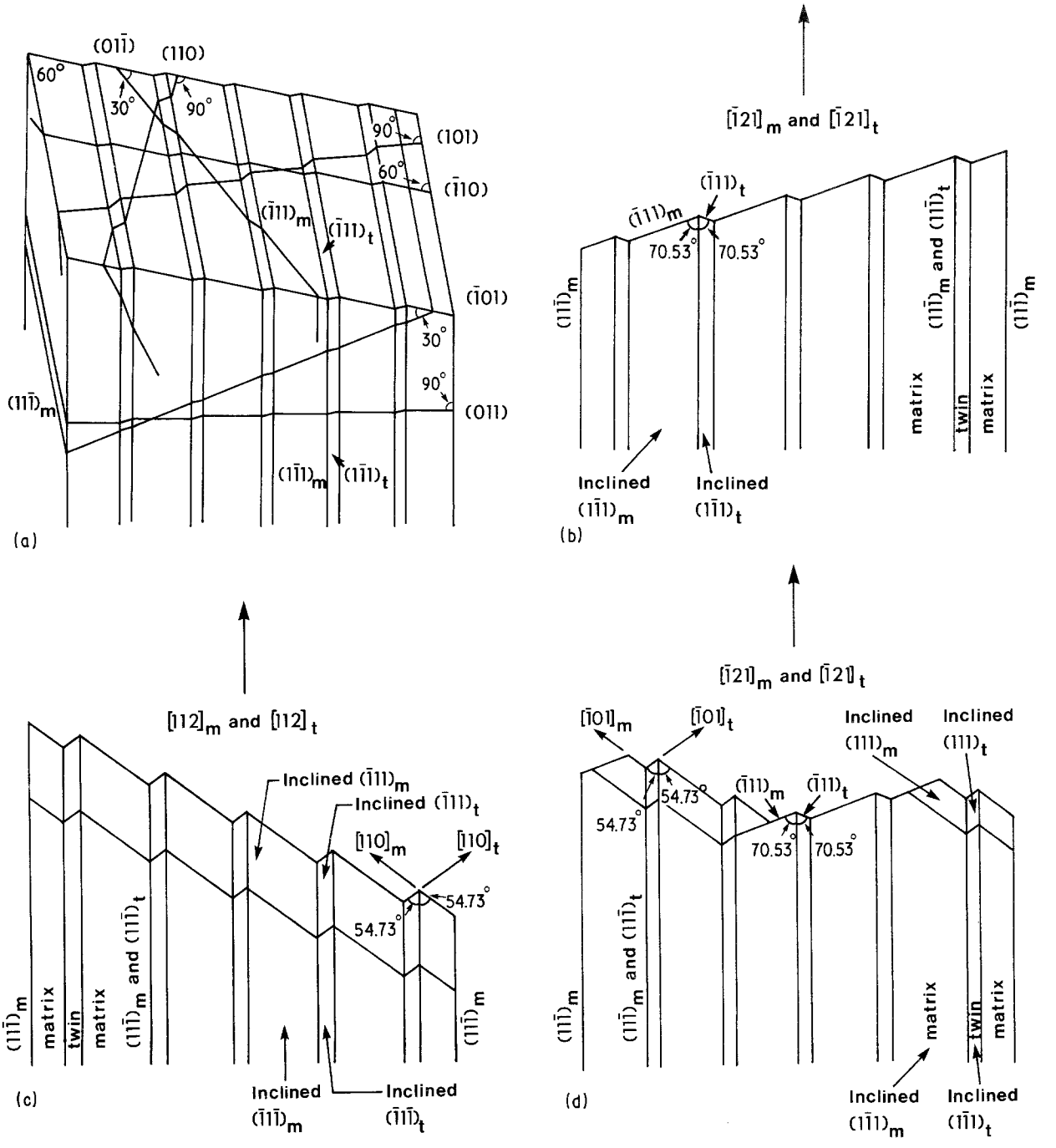

Figure 8 ⟨1 1 0⟩ projections through a three-dimensional branch tip containing thin twins (the suffix m refers to the matrix and t to the twin material). (a) Perspective sketch of the tip showing the thin twins and the six {1 1 0} planes: the twin plane is edge-on only in (1 0 1), ($\bar{1}$ 1 0) and (0 1 1). (b) [1 0 1] projection: both the twin plane (1 1 $\bar{1}$) and the growing interface ($\bar{1}$ 1 1) are perpendicular to the image plane. (c) [$\bar{1}$ 1 0] projection: the twin plane (1 1 $\bar{1}$) is perpendicular but ($\bar{1}$ 1 1) is inclined to the image plane. (d) [1 0 1] projection where the growing interface consists of two {1 1 1} planes, edge-on ($\bar{1}$ 1 1) and inclined (1 1 1): the macroscopic tip profile is wavy.

growth along ⟨1 1 1⟩, Washburn found that microtwins nucleated as soon as the interface moved but no twins formed for a ⟨1 0 0⟩ growth direction. These results were interpreted in terms of ease of atomic bonding. It was assumed that an atom had to form two bonds to become part of the crystalline silicon. A single atom could attach anywhere to a {1 0 0} surface and form two bonds, but on a {1 1 1} surface three atoms had to attach simultaneously to satisfy the bonding criterion. Atomic attachment on {1 1 1} surfaces was facilitated by twin formation because then only two atoms had to be correctly positioned. Furthermore, the microtwins were often nucleated on {1 1 1} faces inclined to the main growth direction. These observations may be relevant to the solidification of modified silicon. The spine may grow along a ⟨1 0 0⟩ or ⟨1 1 0⟩ by random atom addition. As growth proceeds, {1 1 1} facets develop on the sides of the spine and branches nucleate at these facets. Provided thermal and chemical conditions in the adjacent melt are suitable, the branches grow outwards and the {1 1 1} faults are nucleated to aid growth by the re-entrant edge mechanism and lateral microscopic growth. The short faults in the spine may then be interpreted as sites which did not develop into full branches due to competition with the aluminium phase.

From the above considerations we conclude that the thin {1 1 1} faults are connected with the growth of modified silicon and are not artefacts. Although there

is circumstantial evidence that the faults aid growth, there is no direct proof. For growth aided by a twin re-entrant edge mechanism, the growth front is traditionally expected to be both macroscopically and microscopically faceted [4, 6]. But the considerations discussed above show that it is possible for these re-entrant edges to aid growth without macroscopic faceting. By providing nucleation sites for riser growth in the Lateral Microscopic and Perpendicular Macroscopic Growth models [11], thin twins may aid solidification but produce a macroscopically curved solid–liquid interface on which the risers may be microscopically curved as well. Therefore the absence of macroscopic faceting is not necessarily a contra-indication of twin re-entrant edge growth.

5. Conclusions

1. Thin {1 1 1} faults are present in modified silicon dendrites and are a mixture of very thin twins and stacking faults, the inter-twin spacing being ten times the twin width. Thick twins, large enough to form discrete twin spots, are virtually absent from the modified silicon.

2. The thin twins and stacking faults are not artefacts of specimen preparation and are unlikely to be deformation twins formed by thermal compressive stresses.

3. The shape of the solidified interfaces at branch tips provides neither conclusive proof nor contra-indications for twin re-entrant edge growth.

4. The thin faults apparently aid growth but the resultant interfaces are not macroscopically faceted. The faults may help by facilitating Lateral Microscopic Growth in which microscopic faceting exists on the terraces or treads, but the macroscopic outline of the interface is non-faceted.

Acknowledgements

This study began at Comalco Research Centre, Thomastown, Australia, while one of the authors (H.W.K.) was a visiting scientist there. The specimens were provided through the cooperation of various personnel at Comalco. The high-resolution microscopy was carried out at the Microstructural Sciences Laboratory, National Research Council of Canada, in Ottawa. The work was funded by grants from the Natural Sciences and Engineering Research Council of Canada.

References

1. S. C. FLOOD and J. D. HUNT, *Metal Sci.* **15** (1981) 15.
2. D. C. JENKINSON and L. M. HOGAN, *J. Cryst. Growth* **28** (1975) 171.
3. H. A. H. STEEN and A. HELLAWELL, *Acta Metall.* **20** (1972) 1.
4. R. S. WAGNER, *ibid.* **8** (1960) 57.
5. S-Z. LU and A. HELLAWELL, *J. Cryst. Growth* **73** (1985) 316.
6. M. SHAMSUZZOHA and L. M. HOGAN, *Phil. Mag. A* **54** (1986) 459.
7. D. J. D. THOMAS, *Phys. Status Solidi* **3** (1963) 2261.
8. R. STICKLER and G. R. BOOKER, *Phil. Mag.* **8** (1963) 859.
9. D. BROOKSBANK and K. W. ANDREWS, *J. Iron Steel Inst.* **207** (1969) 474.
10. K. YASUTAKE, J. D. STEPHENSON, M. UMENO and H. KAWABE, *Phil. Mag. A* **53** (1986) L41.
11. R. A. FREDERICK and G. A. ROZGONYI, *J. Cryst. Growth* **70** (1984) 335.
12. E. BAUSER and H. P. STRUNK, *ibid.* **69** (1984) 561.
13. J. WASHBURN, in Proceedings of the Materials Research Society Annual Meeting on Defects in Semiconductors, Boston, USA, November 1980, edited by J. Narayan and T. Y. Tan (North-Holland, New York, 1981) p. 209.

Received 2 March
and accepted 29 April 1987